Applied Geochemistry 206 (2026) 106890

Contents lists available at ScienceDirect

Applied Geochemistry

journal homepage: www.elsevier.com/locate/apgeochem

A simple, field-compatible method for accurate pH measurement in hypersaline brines

Paz Nativ *, Gordon D.Z. Williams, Avner Vengosh

Division of Earth and Climate Sciences, Nicholas School of the Environment, Duke University, Durham, NC, USA

ARTICLE INFO

Editorial handling by Elisa Sacchi

Keywords:
Lithium Brine
Hypersaline
pH
Pitzer
PHREEQC
Field geochemistry

ABSTRACT

Accurate pH determination in hypersaline brines is essential for reliable geochemical modeling and simulation, particularly for processes such as direct lithium extraction, carbonate precipitation potential calculations, brine reinjection assessments, and related applications. However, standard pH electrode calibration techniques may produce significant errors in concentrated brines due to elevated liquid junction potential (LJP) and ion interactions with the electrode's glass membrane. Here, we present a robust, field-compatible method for accurate pH measurement in high salinity brines, using standard combined glass pH electrodes and titration-based calibration with tailored buffer solutions. The technique integrates an online PHREEQC (Pitzer model) based software to prepare custom buffer solutions and calibration curves, enabling the re-analysis of field data for correct pH detection. The method was evaluated using data from 16 hypersaline brines across the full evaporation sequence of a lithium production plant in the Salar de Uyuni of Bolivia. pH values obtained using the new method resulted in substantially improved agreement between PHREEQC-simulated and measured total alkalinity compared to standard pH calibration. While simulations based on standard pH calibration showed increased scatter and large errors with increasing ionic strength (up to >95% in total alkalinity simulations), applying the new method reduces these errors to within ±10% across the entire salinity range. This approach provides a simple, generic, low-cost, and effective tool for improving the pH measurement and chemical characterization of hypersaline brine.

1. Introduction

pH is a parameter of high importance for water analysis and assessing water acidity, mineral precipitation potential (PP) or saturation index (SI) for solids, reduction-oxidation (RedOx) potential, and the saturation state of various gases (Benjamin, 2002; Birnhack and Lahav, 2018; Charlton and Parkhurst, 2011; George et al., 2014). pH is a derivative parameter and must be coupled with other conservative parameters such as alkalinity, total concentrations of weak acid systems and ions, ionic strength (I, expressed in units of molar "M", mol/L or molal "m", mol/kgw), and temperature.

The chemical composition of brines from different sources is a subject of growing interest for harvesting energy using geothermal water (Sharmin et al., 2023; Soltani et al., 2021); metal extraction from brines such as lithium (Khalil et al., 2022; Mojid et al., 2024; Tabelin et al., 2021), rubidium (Dagan-Jaldety et al., 2023; Xing et al., 2021), and rare earth elements (REE) (Xie et al., 2023); assessment of acid mine drainage and oil and gas produced waters (Blondes et al., 2023); lithium brine geochemistry from closed-basins (Williams and Vengosh, 2025; Williams et al., 2025); and carbon capture injection wells for CO_2 geologic sequestration (Celia et al., 2015; Ehlig-Economides and Economides, 2010; Ellis et al., 2010; Rosenbauer et al., 2005; Wigand et al., 2008). These topics have shown a steady increase over the past two decades, with more than 390 publications on brine chemistry alone in 2024 (Scopus search, keywords: brine, chemical, composition) ("Scopus - Analyze search results," 2025).

However, in hypersaline brines (brines with a total dissolved solids (TDS) value higher than 70 g/L or about twice the salinity of seawater (Shah et al., 2022)), the measured pH may not be a direct indication of the proton concentration, as is commonly assumed in less saline solutions, due to the extremely high proton activity coefficient (Benjamin, 2002; Dickson, 1984; Müller et al., 2018; Papadimitriou et al., 2016; Sass and Ben-Yaakov, 1977). This may lead to low and less accurate pH measurements of brines, resulting in, among other things, incorrect evaluation of precipitation potential for different solids or gases, which are highly dependent on accurate pH analysis (Golan et al., 2014; Nativ

* Corresponding author.
E-mail address: paznativ@gmail.com (P. Nativ).

https://doi.org/10.1016/j.apgeochem.2026.106890
Received 24 February 2026; Received in revised form 26 April 2026; Accepted 12 May 2026
Available online 18 May 2026

et al., 2026; Nir et al., 2014). Therefore, analysis of chemical properties, such as calcite precipitation potential, weak acid speciation, RedOx potential, and other pH-dependent parameters, requires an accurate and reliable pH measurement method under challenging hypersaline brine conditions (Nativ et al., 2026).

One field of the new technologies for lithium extraction is direct lithium extraction (DLE), which can be used with both low- and high-grade brines (e.g., aluminum hydroxide or manganese oxide ion sieves or sorbents (Saleem et al., 2025; Stringfellow and Dobson, 2021)). The efficacy and efficiency of such DLE technologies have a direct relation to the solution pH (recommended pH range of 5-9). This means that accurately characterizing the chemical composition of the solution is crucial for the choice of the extraction method. Another example is the calcium carbonate precipitation potential (CCPP) or SI, which is important for evaluating the fate of spent brines upon reinjection back into the underlying aquifer in the salar systems, aiming to avoid rock dissolution and/or reduced permeability that could cause sink-holes and property damage (Williams and Vengosh, 2025). Determining the correct pH is also critical for CO_2 sequestration into deep saline aquifers, as pH typically drops when CO_2 dissolves in water, causing the aquifer to become corrosive, potentially impacting the hosting rock water-rock interactions (Ellis et al., 2010; Rosenbauer et al., 2005; Wigand et al., 2008). Nir et al. (2014) showed that pH measurements for CCPP calculations at increased ionic strength above seawater (I > 0.7 M) have significant errors when using standard procedures for pH measurements.

Overall, accurately measuring pH in hypersaline brines is challenging, and various approaches have been proposed to improve accuracy, showing an error range of 0.03-0.15 pH units for ionic strengths of 0.7-10 M (Golan et al., 2014; Nir et al., 2014). These are often complex methods, time-consuming, and/or require special analytical equipment. To perform a pH analysis in these non-ideal conditions, the measuring technique, its limitations, and merits must be fully understood. In this study, we propose a simple and robust method to accurately analyze the pH of hypersaline brines (I > 6 M) using a standard combined glass pH electrode calibrated with a custom curve, rather than specific calibration points, made with a simple titration-based method (Buck et al., 2002; Nir et al., 2014). We use this approach and demonstrate that it can be used with new and archived field pH measurements. To make this entire process readily approachable, a PHREEQC/Pitzer-based Excel software has been developed and is available for download in the supplementary section, allowing for easy calculations and analysis of titration results.

1.1. Fundamentals of pH measurement using a combined glass electrode

A combined pH electrode typically consists of a cell containing two reference electrodes separated by a salt bridge and a hydrogen ion (H_3O^+ or H^+) sensitive glass membrane, as illustrated in Fig. 1. The pH electrode measures the electrical potential gradient across the glass membrane that develops from ionic exchange at the glass-solution interface, with a linear correlation to proton activity (Equation (1)).

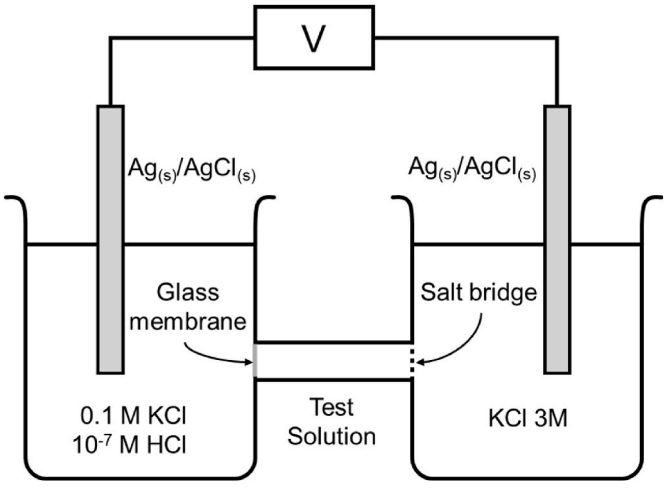

Fig. 1. Electrochemical scheme representation of a combined pH electrode.

When two electrolyte solutions with different compositions of ions or concentrations are separated by a selective barrier, such as a membrane or dense porous medium, an electrical potential develops at the interface of the two solutions (Buck et al., 2002; Graham et al., 2013; Hamann et al., 2007). In a combined pH electrode, this potential is referred to as the LJP and is developed over the salt bridge of the Ag/AgCl reference electrode (Fig. 1).

The measured electrical potential (typically measured in mV) of the cell is linearly correlated with the pH (or the activity of H^+) of the test solution according to the following Nernst-derived equation (the slope under standard conditions is 59.6 mV/pH):

$$E = E_0 + \ln(10)\frac{RT}{F}\cdot pH \quad (1)$$

where E is the cell electrical potential (Volt); E_0, the standard potential difference of the cell (V); R, gas constant (Joule·mol^{-1}·K^{-1}); F, Faraday constant (Coulomb·mole^{-1}); and T, temperature (K). E_0 also includes the LJP across the salt bridge between the reference electrode and the measured solution, and its value is empirically verified by using pH buffer solutions with known pH values.

pH measurements at low ionic strength (I < 0.1 M) are well established, with accepted definitions and procedures (Buck et al., 2002). The standard method for pH measurement typically includes using two or more calibration buffer solutions with known pH. The pH electrode's electrical potential output for each buffer solution is recorded, and a linear regression equation is produced, with the pH as the dependent variable and the recorded mV as the independent variable. As the reference electrode connected to the glass membrane is immersed in a pH 7 solution (Fig. 1), the measured electrical potential of a pH 7 buffer solution is approximately zero, since almost no proton gradient should develop under these conditions.

When measuring pH in high salinity solutions (I > 0.1 M (Buck et al., 2002)), several parameters may cause erroneous reading: (i) Different LJP due to high concentration gradient of the test solution compared to the pH calibration buffers, (ii) Interaction of ions with the proton selective glass membrane may also cause shifts in the electrical potential reading, and (iii) High viscosity may change the diffusion and mobility of ions in the solution and in the LJP, allowing for additional changes in the potential reading (Golan et al., 2014; Graham et al., 2013; Marcus, 1989; Nir et al., 2014).

The change in the LJP is thought to be the major contributor to the error in pH readings of high-salinity solutions (Ben-Yaakov and Sass, 1977; Golan et al., 2014; Knauss et al., 1990; Marcus, 1989; Nir et al., 2014). Several methods have been proposed to address this issue: using a deconstructed pH electrode cell with two standalone ion-selective electrodes (ISE) without the salt bridge (Fig. 1) (Ben-Yaakov and Sass, 1977; Golan et al., 2014; Knauss et al., 1990; Marcus, 1989); applying titration methods (Mesmer, 1991); and various remote and in-situ sensing methods (Avolio et al., 2022; Easley and Byrne, 2012; Millero et al., 2009). The absolute difference between the pH values obtained by the regular and the different proposed methods mentioned above ($|pH_{regular} - pH_{new\text{-}method}|$) ranges from 0.05 to 0.2 pH units, with ionic strength values as high as 10 m (the Dead Sea (Golan et al., 2014),).

Dagan-Jaldety et al. (2025) and Nir et al. (2014) proposed to address the challenge of pH measurement in high salinity solutions using custom-made pH buffer solutions (at I < 2 M), allowing the calibration of the pH electrode to be done in close to real-life conditions, as well as using the PHREEQC software (modified Pitzer and SIT databases) to simulate the pH buffers' chemical composition and determine their accurate pH.

For computer simulation, the Pitzer model is regarded as the best available choice when modeling high salinity solutions. Standard models such as Debye-Hückel theory or the Bates-Guggenheim convention only work well at low ionic strengths (I < 0.1 M), while in concentrated brines, the models' simplifying assumptions are no longer valid. The Pitzer model, however, considers specific ion-solvent interactions, which become crucial for accurate simulation at high ionic strengths.

To create custom pH buffer solutions, weak acid systems must be modeled. This is a major limitation of the Pitzer model, which only includes a few weak acid systems (i.e., H_2CO_3, H_4SiO_4, H_3BO_3). To expand the Pitzer model for the addition of weak acid systems for custom pH buffer calibration solution preparation (such as phthalic acid or phosphoric acid (Nir et al., 2014)), ion interaction parameters must be fitted to experimental data, typically osmotic or activity coefficients, using methods like least-squares analysis. These parameters, often compiled or re-evaluated from the literature (Chan et al., 1995; Covington and Ferra, 1994; Ferra et al., 2009; Millero, 2009; Pitzer, 1973; Spitzer et al., 2011), allow for accurate modeling of complex solutions. Such parameters are, however, often limited in applicability due to a lack of data on divalent ion interactions, and thus the Pitzer model can only be expanded to model solutions with dominantly sodium and potassium ions (Moog et al., 2015).

When characterizing hypersaline solutions (TDS >70 g/L), such as the brine from lithium evaporation ponds (Williams et al., 2025, 2026) or oil and gas produced waters (Blondes et al., 2023), elements such as magnesium, calcium, and iron, rather than sodium and potassium, may be (or become) the dominant cations. As a result, only the unmodified Pitzer database can be used in PHREEQC to accurately calculate ion activities, making the task of creating a custom pH buffer solution for these hypersaline brines highly challenging.

2. Materials and methods

2.1. Simulation tools

The PHREEQC software (Ver. 3.8.6.17100) (Charlton and Parkhurst, 2011) and the Pitzer database (the standard unmodified database provided with PHREEQC) were used for all solution simulations. A PHREEQC-powered software was written for the suggested titration method and is available online (https://peel.twix.technion.ac.il/research/resources/). A sample input syntax for PHREEQC, to simulate the titration data, is provided in Appendix A.

2.2. pH measurement setup

For pH measurements, a Metrohm combined pH glass electrode (3 M KCl) was used with a Metrohm 913 pH meter.

All pH measurements and titrations were conducted at 25 °C, using a water bath. The pH meter applies temperature correction to the electrode response, ensuring consistency of the measured potential.

Furthermore, temperature effects on solution thermodynamics (equilibrium constants, ion activities, and species distribution) are not corrected by the pH meter and must be accounted for in PHREEQC simulations. Accordingly, the simulation temperature should match the intended application: the laboratory temperature for comparison with measured total alkalinity (TA), or the field temperature for in-situ speciation analysis.

All chemicals were of analytical grade and were dried in a 50 °C oven before use; all solutions were prepared using Deionized water (DIW).

2.3. Brine sample chemical composition

16 brine samples from the Salar de Uyuni (SDU) lithium production plant in Bolivia were selected to evaluate and verify the method, using data reported in (Williams et al., 2025). Brine samples B1.0–5.0, 8.0, 10.0, & 11.0 are natural brines, and samples B1.1–1.8 are brines collected from sequential evaporation ponds (numbered in order) used for lithium extraction. The chemical and physical composition, measured total alkalinity (TA), and simulated TA using PHREEQC are presented in Table 1.

2.4. Titration protocol and calibration curve

The protocol for producing the custom pH buffer solution and the titration method for producing the pH calibration curve are described below.

For all measurements, the electrode potential was considered stable when variation was less than ±0.5 mV over a 30 s interval, with a minimum equilibration time of 2 min at each titration step. At least triplicate titrations are recommended to ensure reproducibility and high-quality calibration ($R^2 > 0.98$; see Table B1).

2.4.1. Reagents, equipment, and sample data

- Sample chemical and physical compositions: major cations, sulphate, boron, chloride, total dissolved solids (TDS), and specific density.
- A 0.4 M Boric acid, and 1 M NaOH solutions.
- The following salts (analytical grade, showing anhydrous form, hydrated salts can also be used): $MgCl_2$, $CaCl_2$, NaCl, Na_2SO_4, $MgSO_4$, LiCl and KCl.
- Basic water laboratory equipment.
- A combined pH glass electrode with a pH meter capable of displaying the measured electrical potential (U - in mV).

2.4.2. Protocol

Step 1 - custom pH buffer solution preparation (by using the online software)

- Open the software web page (link in section 3.1) and fill in the sample chemical and physical data in the “Sample composition” table (marked 1).
- Choose the relevant salt's hydrated state (based on the salts available to you) in the “Salt hydration state” table (marked 3).
- A recipe for the custom buffer is calculated in the bottom table titled “Buffer recipe - per 1 kg H_2O”. All data is in mmol or g to 1 kgw. Note that the mass of required water changes due to the hydration of the salt.
- Mix the salts and water, monovalent salts should be added prior to the addition of divalent salts to improve dissolution efficiency. After complete dissolution, filter the solution using a 0.45 μm filter and keep the buffer solution at 25 °C.

Step 2 - titration curve simulation and working details

- In the “Titration setup” table (marked 2), enter the data of your acid, base, and sample solutions concentrations and volumes.
- For a 25 mL sample, 4-5 mL of boric acid is required to allow for a high buffer capacity. Please adjust the volume accordingly (for example, if a 50 mL sample is used, 10 mL of 0.4 M boric acid is needed, and so on).
- Choose the strong base volume, between 1 and 2 mL, and press the “Run simulation” button to update the “Titration results” table (marked 6) and Figs. 7–9.
- Aim at reaching results where the B4/B3 ratio equals close to unity, and with at least 2-3 titration steps before and after said point in the titration (see results section 3.1 Custom pH buffer solution definition, for details and explanations).

Step 3 - titration and results analysis

- Use standard water lab titration procedure (magnetic stirrer, burette, etc.).
- Add to the buffer solution the required volume of the boric acid.
- Place the pH electrode (set the output to U - mV) in the buffer solution and wait until the reading stabilizes.

Table 1
Chemical composition of the natural (shaded) and evaporation ponds brines from the Salar de Uyuni (SDU) lithium production plant. Data from Table S1 in (Williams et al., 2025).

Name	Na^+	K^+	Li^+	Mg^{2+}	Ca^{2+}	SO_4^{2-}	B^-	Cl^-	Br^-	Density	I	pH*	TA	TA**
	g/L	g/L	g/L	g/L	g/L	g/L as S	g/L	g/L	g/L	kgs/L	M		meq/kgs	meq/kgs
B1.0	88.8	20.6	1.0	20.5	0.26	9.6	1.2	189.0	0.11	1.229	7.22	6.84	22.4	21.2
B2.0	73.5	21.7	1.4	28.0	0.28	8.1	1.4	193.0	0.17	1.228	7.49	6.69	27.2	26.3
B3.0	91.6	17.3	0.8	16.3	0.35	7.9	1.0	185.7	0.10	1.221	6.70	7.00	18.3	17.2
B4.0	99.4	16.1	0.7	14.3	0.41	7.6	0.9	181.9	0.07	1.221	6.62	7.09	16.6	15.2
B5.0	72.2	21.3	1.4	27.5	0.32	8.3	1.5	191.4	0.17	1.227	7.39	6.69	28.4	27.3
B8.0	95.3	18.2	0.8	17.4	0.39	7.9	0.9	187.8	0.09	1.222	6.96	7.00	18.1	17.0
B10.0	74.8	21.9	1.3	27.2	0.33	8.0	1.3	192.7	0.16	1.225	7.46	6.66	24.1	22.3
B11.0	81.1	19.5	1.1	21.9	0.34	7.6	1.2	190.9	0.14	1.224	7.03	6.75	21.2	18.9
B1.1	74.6	25.3	1.3	26.7	0.33	11.2	1.5	189.8	0.16	1.236	7.58	6.69	28.4	26.4
B2.2	69.7	28.4	1.5	30.6	0.30	11.9	1.7	190.3	0.18	1.238	7.92	6.63	32.2	30.9
B1.3	53.1	35.8	1.9	40.0	0.18	14.5	2.2	191.4	0.24	1.250	8.61	6.37	40.8	37.8
B1.4	18.9	22.7	4.0	67.4	0.13	15.4	4.4	214.3	0.49	1.272	10.42	5.39	81.5	75.5
B1.5	23.6	27.4	4.2	64.9	0.14	15.7	4.1	218.7	0.51	1.269	10.55	5.51	80.0	77.4
B1.6	7.5	11.8	5.7	84.8	0.12	9.5	5.1	255.8	0.79	1.286	11.82	4.63	76.5	87.4
B1.7	2.1	1.1	5.7	107.2	0.03	10.0	5.0	290.0	1.01	1.330	13.69	3.50	63.3	51.8
B1.8	1.7	0.6	6.2	112.1	0.03	7.5	7.8	326.6	1.75	1.341	14.45	3.18	62.0	121.4

* pH analyses were done using regular pH calibration buffers.

** TA calculated using PHREEQC simulation, using the chemical composition and measured pH.

- Add NaOH in the calculated volume titrations from Step 2.
- Record the mV output for each titration step.
- Place the mV data along with the pH data from the "Titration results" table.
- Take the five titration points with the highest buffer capacity, i.e., the titration points for which the B4/B3 ratio is closest to unity, with two titration points before and after that point. Produce a calibration curve with the calculated pH on the y-axis and the measured mV on the x-axis. For example, if the B4/B3 ratio is close to unity after 7 titration steps, point 7 is taken as the middle point, together with points 5 and 6 before it, and points 8 and 9 after it.
- The linear regression is calculated automatically in Figure 7, "pH Calibration - mV vs. calculated pH".

Step 4 - pH analysis and re-analysis of previous data

- Use the original brine sample and measure the mV output.
- Use the results with the produced function from step 3 to calculate the sample's pH using the new method.
- To re-analyze a sample's pH (if the sample is not available), use standard pH buffer solutions to calibrate the electrode, produce a calibration curve function, and derive the mV data from the recorded pH. Use the derived mV data in the custom buffer calibration function to recalculate the pH.

3. Results and discussion

3.1. Custom pH buffer solution definition

A critical requirement for a pH buffer solution is that its pH value must fall within a range of high buffer capacity, to allow for accurate pH reading and stabilization of the pH electrode output. Buffering capacity or buffering intensity (β) is defined as the change in pH due to the addition of acid or base. The equation for calculating β (with acid addition) is shown in Equation (2):

$$\beta = -\left(\frac{dC_a}{dpH}\right) \tag{2}$$

where C_a is the acid concentration (M).

Buffer capacity is inversely related to the change in pH; minor changes in pH correspond to higher buffer capacity, and vice versa. A buffer capacity curve can be constructed by titrating an acid or base and plotting β versus pH. When weak acid systems are present in the solution, a high buffer capacity is observed at pH = pK (see Equation (3)), and high values are present at both high and low pH values due to the water system's buffering capacity (Benjamin, 2002; Lahav and Birnhack, 2019). In this study, buffer capacity (β) is derived from PHREEQC simulations of the titration process and is not based on empirical measurements. Typically, single or several weak acids are used to prepare a pH buffer solution, such as phosphoric acid, phthalic acid, citric acid, and boric acid, among others. pH Buffer solutions prepared with weak acids that have a gas phase species (such as ammonia, carbonic, or sulfide weak acid systems) will be less stable over time due to gas-liquid equilibrium, making these types of acids an undesirable choice. In the Pitzer model, boric acid is the only weak acid system present without a gaseous phase (Equation (3)), making it the sole candidate for a custom pH buffer solution, as divalent ions must be accounted for in a generic brine simulation.

$$B(OH)_3 \leftrightarrow B(OH)_4^- + H^+, k = 10^{-9.239} \tag{3}$$

The structural units of boric acid ($B(OH)_3$, trigonal planar, defined here as "B3") and the borate ion ($B(OH)_4^-$, tetrahedral, defined here as "B4") can polymerize to form polyborate ions (Mesmer et al., 1972; Zhou et al., 2011), along with divalent ion complexes (Williams et al., 2025). For all calculations of buffer capacity of the custom pH buffer calibration solution using the boric weak acid system, B4 and B3 were used (their values represent a sum of all ionic complexes for each) instead of the free weak acid species ($B(OH)_3$ and $B(OH)_4^-$; Fig. 2). For further details and explanations on the Boric acid system and polyborate complexes, we refer readers to (Williams et al., 2025).

In Fig. 2, two simulated buffer capacity curves are shown, with ionic background of deionized water (DIW) and of a lithium evaporation pond (Table 1, sample B1.8; (Williams et al., 2025; Williams et al., 2025), and a total boron concentration of 50 mM, showing the high buffer capacity at the point where B4 concentration equals the B3 species concentration (or the molar ratio between B4 and B3 is close to unity) (Williams et al.,

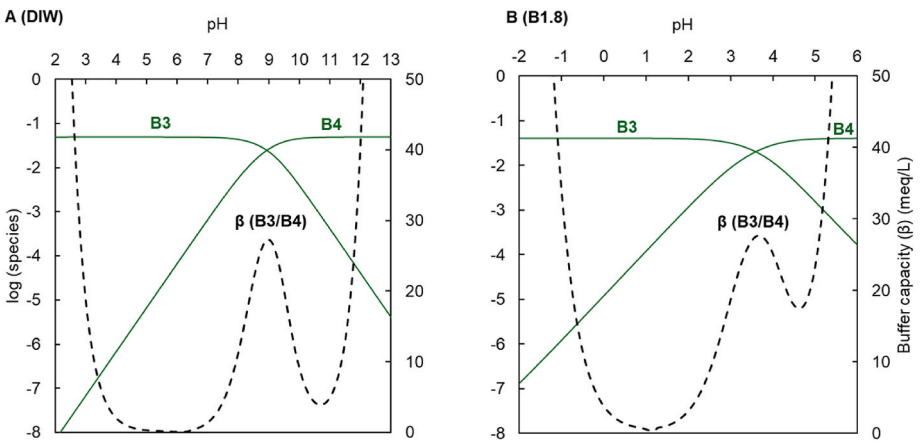

Fig. 2. B3 and B4 boron species distribution (green lines) and the calculated buffer capacity (β) curve (dashed black line), with DIW (I < 0.1 M) and pond sample B1.8 (I > 14 M) (Table 1) ionic background (A and B, respectively). (Pitzer database, $[B]_T = 50$ mmol/L). (For interpretation of the references to colour in this figure legend, the reader is referred to the Web version of this article.)

2025). The shift in the pK value of the hypersaline source relative to the DIW background arises from changes in solution ionic strength and the high proton activity coefficient under these conditions, which results in a low pH (both calculated and measured). Additionally, the increase in buffer capacity at pH values above 5.5 in the high-salinity example is primarily due to magnesium complexation with hydroxide ions. The condition $B_4/B_3 \approx 1$ corresponds to equal concentrations of boric acid structures and borate structures and therefore occurs near the apparent pK_a of the boric acid system. This point defines the region of maximum buffer capacity. Under hypersaline conditions, the apparent pK_a is shifted due to ionic strength effects.

In the proposed new method presented in this study, a single pH buffer solution is used, as only the boric system is available in the unmodified Pitzer model, unlike typical pH calibration methods, which use two or more pH buffer solutions to produce the calibration curve. At least five titration points with high buffering capacity are selected from the titration curve data. High buffering capacity ensures a low error in pH reading and good stabilization of the pH electrode output. As explained in Section 3.4.2 (steps two and three), the value of the titration point where the B4 to B3 ratio is close to unity is selected, along with at least four additional points, before and after this point. This ensures that the selected calibration points are within a pH range in the custom buffer solution with high buffering capacity (see Fig. 2B).

3.2. Re-analysis of field data

To assess the accuracy of the proposed method, 16 data points of brines from evaporation ponds in the SDU lithium production plant were reanalyzed using published data (Williams and Vengosh, 2025; Williams et al., 2025). The TA of the brine samples was measured using the Gran titration method (Gran, 1952; Lew et al., 2009). In this method, the analysis is not sensitive to the absolute pH value; as a linear regression of the titration data is used. Therefore, the TA value can be used to assess the validity of the proposed method, as it is almost pH-independent. 16 custom pH buffer solutions were prepared from the chemical and physical data in Table 1, and the new method was employed to create 16 calibration curves (n = 3). Using a standard pH calibration curve, the mV values of the samples were calculated, and their values were plugged into the new calibration curves to calculate new pH values for each of the 16 data points. The original (standard) and the new method's calibration curve data, and pH values are presented in Table B1, along with the standard deviations and coefficients of determination. Across all samples, the calibration slopes of the new method remain close to the theoretical value (Eq. (1)), whereas the intercept values vary with brine chemistry.

Williams et al. (2025) showed that the total alkalinity (TA) simulated by PHREEQC (Pitzer database) agrees with the measured TA and pH of the SDU brines (Table 1). The exceptions are the highly saline evaporation ponds (I > 10 M), which have measured TA values that are considerably different from those of the simulated values. TA is a function of the total concentration of the weak acid systems and pH, using converted equilibrium constants for the temperature and ionic strength (Benjamin, 2002; Lahav and Birnhack, 2019; Nir et al., 2014). Therefore, when simulating a sample solution from chemical composition data (total concentrations) and measured pH, a higher pH will increase the calculated TA value, and vice versa.

Fig. 3 summarizes the results of the new pH calibration method compared to the standard calibration of the 16 samples tested. In Fig. 3A, TA values from PHREEQC simulations using pH values obtained by the new method more closely follow a 1:1 relationship with empirically measured TA, whereas PHREEQC simulations based on standard pH calibration exhibit greater scatter and pronounced deviations at higher ionic strength. In particular, standard calibration yields a substantial overestimation of TA in extreme ionic strength brines with pH deviating from circumneutral. Sample B1.8 has the highest ionic strength in the dataset (I ≈ 14.5 M) and exhibits a large discrepancy between the standard and recalculated pH values (Table B1). This is shown in the TA comparison, where standard pH calibration results in a 95.9% simulation error, compared to 1.9% using the recalculated pH from the proposed method (Table B2). Fig. 3B shows the absolute error in PHREEQC simulated TA using standard and the new method pH values as a function of ionic strength. Errors associated with standard pH calibration increase with ionic strength and display large variability, including extreme values for the highest-salinity brine samples. Of the 16 samples analyzed, one brine sample (pond B1.6) showed an absolute TA error of ~30% when the new calibration method was applied. This error may arise from analytical uncertainty in the reported chemical composition or from cumulative modeling uncertainty under extreme ionic strength conditions. In contrast, errors obtained with the new method remain comparatively low and bounded across the investigated salinity (ionic strength) range, indicating improved robustness under increasingly complex and challenging conditions of the hypersaline brines. Error-based statistical metrics indicate a substantial improvement in the simulation of the TA value using the proposed method. The mean absolute error (MAE), root mean square error (RMSE), and mean absolute percentage error (MAPE) were reduced from 6.72, 15.53, and 13.0% (standard calibration) to 2.86, 6.31, and 5.02%, respectively (Table B2). Errors associated with standard pH calibration show a strong dependence on brine composition, such as higher error in Li-dominant brines and lower error with Na-dominant brines. In contrast, errors

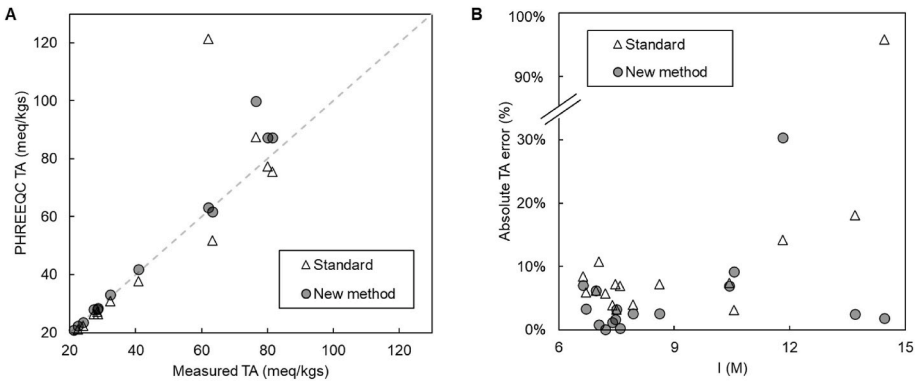

Fig. 3. (A) Comparison between empirically measured TA and PHREEQC simulated TA in brines collected from evaporation ponds in the Salar de Uyuni, Bolivia. Open triangles represent simulations based on standard pH calibration, and filled circles represent simulations using the new titration-based pH calibration method presented in this study. The dashed line indicates a 1:1 relationship, and (B) Absolute TA simulation error as a function of ionic strength. Standard pH calibration exhibits increasing scatter and large deviations at higher ionic strength, including extreme errors in the most concentrated brines, whereas the new method maintains bounded and generally lower errors across the investigated salinity range.

obtained using the proposed calibration method exhibit substantially weaker correlations with cation ratios, indicating reduced sensitivity to brine chemistry (Table B2).

4. Conclusions

This study presents and verifies a new pH measurement method in hypersaline brines. The technique differs from previous procedures in that it uses a standard combined pH electrode and a source specific buffer solution, combined with a titration derived calibration curve. By using an ionic background similar to the investigated brine, the method accounts for LJP and ion exchange reactions with the glass membrane, which affect the standard pH measurements at high ionic strength. To validate the method, a full sequence of 16 hypersaline water sources from the SDU lithium production plant were re-analyzed. Results demonstrate improvement in pH derived geochemical simulations using the PHREEQC software (Pitzer database) even for extremely high salinity conditions. When standard calibration pH values were used in PHREEQC simulations, calculated TA exhibited increasing scatter and deviation with increasing ionic strength, including extreme overestimation in the most concentrated brines (absolute error >95%). In contrast, using pH obtained from the new method to simulate TA closely reproduced empirically measured TA across the entire ionic strength range, with errors remaining bounded and generally within ±10%, even at extreme ionic strengths of ~15 M.

This approach, which relies on readily available combined pH glass electrodes and simple titration techniques, offers a practical and reliable solution for the field and laboratory analysis of complex hypersaline brines. The method was validated using hypersaline lithium-rich brines and is expected to be applicable to other hypersaline systems (e.g., geothermal reservoirs, oil and gas produced water, acid mine drainage effluents, and natural saline lakes such as the Dead Sea and Great Salt Lake), subject to further validation. The new method enables source-specific pH calibration in an ever-changing geochemical environment.

Funding

This study was funded by the Critical Minerals Hub at Duke University.

CRediT authorship contribution statement

Paz Nativ: Conceptualization, Data curation, Formal analysis, Investigation, Methodology, Project administration, Software, Validation, Visualization, Writing – original draft, Writing – review & editing. **Gordon D.Z. Williams:** Data curation, Investigation, Writing – review & editing. **Avner Vengosh:** Conceptualization, Funding acquisition, Resources, Supervision, Writing – review & editing.

Declaration of competing interest

The authors declare that they have no known competing financial interests or personal relationships that could have appeared to influence the work reported in this paper.

Acknowledgments

The authors would like to thank the Bolivian Ministry of Hydrocarbons and Energy and Yacimientos de Litio Bolivianos (YLB) for authorizing, facilitating, and accompanying the sampling missions at and around the Salar de Uyuni in Bolivia. We thank K. Ledebur (Andean Information Network), who provided invaluable logistical and field support during the sampling campaigns. The authors would also like to thank G.S. Dwyer (Duke), R.C. Hill (Duke), and G.A. Hall (Duke) for aid with analytical methods. We also thank three anonymous reviewers for their thorough and detailed reviews, which have improved the quality of this paper.

APPENDIX A

Sample input syntax for PHREEQC. The data used for this example is presented in Table A1, followed by the PHREEQC input syntax. The composition of pond B1.1, the buffer salt recipe, and the titration data are presented in Table A1.

Table A1
The data used to populate the PHREEQC syntax, showing the chemical composition of pond B1.1 (Table 1), the buffer recipe, salt, and water mass, and the titration setup data.

B1.1 chemical composition		
Ion	Concentration	Unit
Na	74594.0	mg/L
K	25321.5	mg/L
Li	1284.1	mg/L
Mg	26700.9	mg/L
Ca	334.6	mg/L
SO_4	11219.2	mg-S/L
B	1488.8	mg/L
Br	158.2	mg/L
Density	1.2357	kgs/L
TDS	286	g/L
pH	6.69	
Buffer recipe		
Salt	mmol	g
$MgCl_2$	787.81	75.01
$CaCl_2$	8.79	0.98
LiCl	194.80	8.26
$MgSO_4$	368.93	44.41
NaCl	3416.47	199.66
Na_2SO_4	368.93	52.40
KCl	681.93	50.84
H_2O	55510	1000.00
Titration setup		
H_3BO_3	0.4	M
V(sample)	25	mL
V(H_3BO_3)	5	mL
NaOH	1	M
V(NaOH)	2	mL
NaOH steps	0.1	mL/step

PHREEQC input syntax.

```
SELECTED_OUTPUT 1
-molalities     B(OH)3  B(OH)4- B3O3(OH)4-  B4O5(OH)4-2  MgB(OH)4+  CaB(OH)4+
-pH     true

SOLUTION        1
        temp    20
        pH      7
        pe      4
        redox   pe
        units   mol/l
        C(4)    1       CO2(g) -3.370590401
        -water  1       #       kg

REACTION        1
        MgCl2   3.939061182
        CaCl2   0.043957596
        LiCl    0.974021204
        MgSO4   1.84467205
        NaCl    17.08235215
        KCl     3.409646166
        Na2SO4          1.84467205

        200     millimoles      in      1       steps
SAVE    Solution        1
END
USE     Solution        1

REACTION        2
        H3BO3   1
        H2O     138.889
        84.2361004      millimoles      in      1       steps

SAVE    Solution        1
END
USE     Solution        1

REACTION        2
        NaOH    1
        H2O     55.5556
        84.2361004      millimoles      in      20      steps
```

APPENDIX B

Table B1
Calibration parameters for the titration-based pH calibration curves were developed for each brine listed in Table 1. Also presenting the calibration curve data for standard pH buffers (pH 2, 4, and 7). Reported values include the linear regression slope (pH/mV), intercept (pH), associated standard deviations, and coefficients of determination (R^2), n = 3.

Tag	Slope	STDV	Intercept	STDV	R^2	pH	pH
	pH/mV	x10^{-4}	pH	x10^{-3}		Standard	New method
Standard	−0.0171		7.06		0.99992		
B1.0	−0.0166	0.3	7.10	2.5	0.99180	6.84	6.89
B2.0	−0.0163	1.1	7.08	1.3	0.99994	6.69	6.74
B3.0	−0.0166	0.9	7.07	14.6	0.99997	7.00	7.02
B4.0	−0.0164	0.8	7.07	2.8	0.99995	7.09	7.10
B5.0	−0.0172	13.0	7.08	18.2	0.96254	6.69	6.71
B8.0	−0.0165	0.5	7.06	3.7	0.99994	7.00	7.00
B10.0	−0.0163	0.7	7.09	4.7	0.99996	6.66	6.71
B11.0	−0.0167	2.5	7.12	10.7	0.99987	6.75	6.82
B1.1	−0.0163	0.6	7.09	9.1	0.99995	6.69	6.75
B2.2	−0.0163	0.3	7.09	9.4	0.99998	6.63	6.68
B1.3	−0.0162	0.7	7.10	3.0	0.99998	6.37	6.45

(*continued on next page*)

Table B1 (*continued*)

Tag	Slope	STDV	Intercept	STDV	R^2	pH	pH
	pH/mV	$x10^{-4}$	pH	$x10^{-3}$		Standard	New method
B1.4	−0.0161	1.0	7.11	7.9	0.99997	5.39	5.55
B1.5	−0.0161	0.3	7.10	7.7	0.99994	5.51	5.65
B1.6	−0.0163	0.6	7.08	3.4	0.99994	4.63	4.78
B1.7	−0.0171	2.2	7.20	10.8	0.99993	3.50	3.66
B1.8	−0.0167	7.5	6.28	25.0	0.99928	3.18	2.50

Table B2
Relative contributions of monovalent cations (Li, Na, K) to total monovalent cation concentration in the analyzed sources, together with absolute errors in PHREEQC-simulated TA using standard and new pH calibration methods. The table provides supporting information for assessing compositional effects on calibration performance.

Tag	TA - empricial	TA – simulation standard	TA – simulation new method	Li^+ ratio	Na^+ ratio	K^+ ratio	Error	Error
	meq/kgs	meq/kgs	meq/kgs	M/M	M/M	M/M	New method	Standard
B1.0	22.4	21.2	22.4	0.03	0.85	0.12	0.1%	5.7%
B2.0	27.2	26.3	28.1	0.05	0.81	0.14	3.2%	3.2%
B3.0	18.3	17.2	17.7	0.02	0.88	0.10	3.4%	6.0%
B4.0	16.6	15.2	15.4	0.02	0.90	0.09	7.0%	8.4%
B5.0	28.4	27.3	28.0	0.05	0.81	0.14	1.2%	3.9%
B8.0	18.1	17.0	17.0	0.02	0.88	0.10	6.3%	6.3%
B10.0	24.1	22.3	23.7	0.05	0.81	0.14	1.7%	7.2%
B11.0	21.2	18.9	21.0	0.04	0.84	0.12	0.9%	10.8%
B1.1	28.4	26.4	28.3	0.05	0.80	0.16	0.3%	7.0%
B2.2	32.2	30.9	33.0	0.05	0.76	0.18	2.6%	4.0%
B1.3	40.8	37.8	41.8	0.08	0.66	0.26	2.6%	7.2%
B1.4	81.5	75.5	87.2	0.29	0.42	0.29	7.0%	7.4%
B1.5	80.0	77.4	87.4	0.26	0.44	0.30	9.2%	3.2%
B1.6	76.5	87.4	99.8	0.57	0.22	0.21	30.4%	14.2%
B1.7	63.3	51.8	61.7	0.87	0.10	0.03	2.5%	18.1%
B1.8	62.0	121.4	63.2	0.91	0.07	0.02	1.9%	95.9%

Data availability

We have added the data in the appendix, and shared a link to the software website.

References

Avolio, R., Grozdanov, Anita, Avella, Maurizio, Barton, John, Cocca, Mariacristina, De, Falco, Francesca, Dimitrov, Aleksandar, T., Errico, Maria Emanuela, Fanjul-Bolado, Pablo, Gentile, Gennaro, Paunovic, Perica, Ribotti, Alberto, Magni, P., 2022. Review of pH sensing materials from macro- to nano-scale: recent developments and examples of seawater applications. Crit. Rev. Environ. Sci. Technol. 52, 979–1021. https://doi.org/10.1080/10643389.2020.1843312.

Ben-Yaakov, S., Sass, E., 1977. Independent estimate of the pH of Dead Sea brine. Limnol. Oceanogr. 22, 374–376. https://doi.org/10.4319/lo.1977.22.2.0374.

Benjamin, M.M., 2002. Water Chemistry. McGraw-Hill, New York, NY.

Birnhack, L., Lahav, O., 2018. Post-Treatment of desalinated Water-Chemistry, design, engineering, and implementation. Sustainable Desalination Handbook: Plant Selection, Design and Implementation. Elsevier Inc. https://doi.org/10.1016/B978-0-12-809240-8.00008-3.

Blondes, Madalyn S., Knierim, Katherine J., Croke, Mary R., Freeman, Philip A., Doolan, Colin, Herzberg, Amanda S., Shelton, Jenna L., 2023. U.S. Geological Survey National Produced Waters Geochemical Database (ver. 3.0, December 2023. https://doi.org/10.5066/P9DSRCZJ.

Buck, R.P., Rondinini, S., Covington, A.K., Baucke, F.G.K., Brett, C.M.A., Camoes, M.F., Milton, M.J.T., Mussini, T., Naumann, R., Pratt, K.W., Spitzer, P., Wilson, G.S., 2002. Measurement of pH. Definition, standards, and procedures (IUPAC Recommendations 2002). Pure Appl. Chem. 74, 2169–2200. https://doi.org/10.1351/pac200274112169.

Celia, M.A., Bachu, S., Nordbotten, J.M., Bandilla, K.W., 2015. Status of CO_2 storage in deep saline aquifers with emphasis on modeling approaches and practical simulations: status of CO_2 storage in deep saline aquifers. Water Resour. Res. 51, 6846–6892. https://doi.org/10.1002/2015WR017609.

Chan, C.-Y., Eng, Y.-W., Eu, K.-S., 1995. Pitzer single-ion activity coefficients and pH for aqueous solutions of potassium hydrogen phthalate in mixtures with KCl and with NaCl at 298.15 K. J. Chem. Eng. Data 40, 685–691. https://doi.org/10.1021/je00019a034.

Charlton, S.R., Parkhurst, D.L., 2011. Modules based on the geochemical model PHREEQC for use in scripting and programming languages. Comput. Geosci. 37, 1653–1663. https://doi.org/10.1016/j.cageo.2011.02.005.

Covington, A.K., Ferra, M.I.A., 1994. A pitzer mixed electrolyte solution theory approach to assignment of pH to standard buffer solutions. J. Solut. Chem. 23, 1–10. https://doi.org/10.1007/BF00972604.

Dagan-Jaldety, C., Lahav, O., Ben-Asher, R., Saller, G., Oz, S., Nativ, P., 2025. Innovative ammonia harvesting from wastewater: a controlled closed-loop process at high pH for enhanced nutrient recovery. Chem. Eng. J. 503, 158201. https://doi.org/10.1016/j.cej.2024.158201.

Dagan-Jaldety, C., Nativ, P., Cristal, Y.S., Lahav, O., 2023. A prussian-blue analogue (PBA) ion-chromatography-based technique for selective separation of Rb+ (as RbCl) from brines. Water Res., 120757 https://doi.org/10.1016/j.watres.2023.120757.

Dickson, A.G., 1984. pH scales and proton-transfer reactions in saline media such as sea water. Geochem. Cosmochim. Acta 48, 2299–2308. https://doi.org/10.1016/0016-7037(84)90225-4.

Easley, R.A., Byrne, R.H., 2012. Spectrophotometric calibration of pH electrodes in seawater using purified m-Cresol purple. Environ. Sci. Technol. 46, 5018–5024. https://doi.org/10.1021/es300491s.

Ehlig-Economides, C., Economides, M.J., 2010. Sequestering carbon dioxide in a closed underground volume. J. Petrol. Sci. Eng. 70, 123–130. https://doi.org/10.1016/j.petrol.2009.11.002.

Ellis, B.R., Crandell, L.E., Peters, C.A., 2010. Limitations for brine acidification due to SO2 co-injection in geologic carbon sequestration. Int. J. Greenh. Gas Control 4, 575–582. https://doi.org/10.1016/j.ijggc.2009.11.006.

Ferra, M.I.A., Graça, J.R., Marques, A.M.M., 2009. Application of the pitzer model to assignment of pH to phthalate standard buffer solutions. J. Solut. Chem. 38, 1433–1448. https://doi.org/10.1007/s10953-009-9421-4.

Tchobanoglous, George, Franklin, L., Burton, Ryujiro Tsuchihashi, Stensel, H.D., 2014. Wastewater Engineering: Treatment and Resource Recovery. McGraw-Hill Professional, New York, NY.

Golan, R., Gavrieli, I., Lazar, B., Ganor, J., 2014. The determination of pH in hypersaline lakes with a conventional combination glass electrode. Limnol Oceanogr. Methods 12, 810–815. https://doi.org/10.4319/lom.2014.12.810.

Graham, D.J., Jaselskis, B., Moore, C.E., 2013. Development of the glass electrode and the pH response. J. Chem. Educ. 90, 345–351. https://doi.org/10.1021/ed300246x.

Gran, G., 1952. Determination of the equivalence point in potentiometric titrations. Part II. Analyst 77, 661–671. https://doi.org/10.1039/an9527700661.

Hamann, C.H., Hamnett, A., Vielstich, Wolf, 2007. Electrochemistry. Wiley-VCH.

Khalil, A., Mohammed, S., Hashaikeh, R., Hilal, N., 2022. Lithium recovery from brine: recent developments and challenges. Desalination 528, 115611. https://doi.org/10.1016/j.desal.2022.115611.

Knauss, K.G., Wolery, T.J., Jackson, K.J., 1990. A new approach to measuring pH in brines and other concentrated electrolytes. Geochem. Cosmochim. Acta 54, 1519–1523. https://doi.org/10.1016/0016-7037(90)90177-M.

Lahav, O., Birnhack, L., 2019. Aquatic Chemistry, De Gruyter. De Gruyter, Berlin. https://doi.org/10.1515/9783110603958-201.

Lew, B., Cochva, M., Lahav, O., 2009. Potential effects of desalinated water quality on the operation stability of wastewater treatment plants. Sci. Total Environ. 407, 2404–2410. https://doi.org/10.1016/j.scitotenv.2008.12.023.

Marcus, Y., 1989. Determination of pH in highly saline waters. Pure Appl. Chem. 61, 1133–1138. https://doi.org/10.1351/pac198961061133.

Mesmer, R.E., 1991. Comments on "a new approach to measuring pH in brines and other concentrated electrolytes" by K.G. Knauss T.J. wolery, and K.J. Jackson. Geochem. Cosmochim. Acta 55, 1175–1176. https://doi.org/10.1016/0016-7037(91)90171-Z.

Mesmer, R.E., Baes Jr., C.F., Sweeton, F.H., 1972. Acidity measurements at elevated temperatures. VI. Boric acid equilibriums. Inorg. Chem. 11, 537–543. https://doi.org/10.1021/ic50109a023.

Millero, F.J., 2009. Use of the pitzer equations to examine the dissociation of TRIS in NaCl solutions. J. Chem. Eng. Data 54, 342–344. https://doi.org/10.1021/je800387n.

Millero, F.J., DiTrolio, B., Suarez, A.F., Lando, G., 2009. Spectroscopic measurements of the pH in NaCl brines. Geochem. Cosmochim. Acta 73, 3109–3114. https://doi.org/10.1016/j.gca.2009.01.037.

Müller, J.D., Bastkowski, F., Sander, B., Seitz, S., Turner, D.R., Dickson, A.G., Rehder, G., 2018. Metrology for pH measurements in brackish Waters—Part 1: extending electrochemical pHT measurements of TRIS buffers to salinities 5–20. Front. Mar. Sci. 5. https://doi.org/10.3389/fmars.2018.00176.

Mojid, M.R., Lee, K.J., You, J., 2024. A review on advances in direct lithium extraction from continental brines: Ion-sieve adsorption and electrochemical methods for varied Mg/Li ratios. Sustain. Mater. Technol. 40, e00923. https://doi.org/10.1016/j.susmat.2024.e00923.

Moog, H.C., Bok, F., Marquardt, C.M., Brendler, V., 2015. Disposal of nuclear waste in host rock formations featuring high-saline solutions – implementation of a thermodynamic reference database (THEREDA). In: Applied Geochemistry, Geochemical Speciation Codes and Databases, 55, pp. 72–84. https://doi.org/10.1016/j.apgeochem.2014.12.016.

Nativ, P., Williams, G.D.Z., Vengosh, A., 2026. Discrepancies between pH and corrosive indices of hypersaline effluents. Environ. Sci. Technol. Lett. https://doi.org/10.1021/acs.estlett.5c01196.

Nir, O., Marvin, E., Lahav, O., 2014. Accurate and self-consistent procedure for determining pH in seawater desalination brines and its manifestation in reverse osmosis modeling. Water Res. 64, 187–195. https://doi.org/10.1016/j.watres.2014.07.006.

Papadimitriou, S., Loucaides, S., Rérolle, V., Achterberg, E.P., Dickson, A.G., Mowlem, M., Kennedy, H., 2016. The measurement of pH in saline and hypersaline media at sub-zero temperatures: characterization of Tris buffers. Mar. Chem. 184, 11–20. https://doi.org/10.1016/j.marchem.2016.06.002.

Pitzer, K.S., 1973. Thermodynamics of electrolytes. I. Theoretical basis and general equations. J. Phys. Chem. 77, 268–277. https://doi.org/10.1021/j100621a026.

Rosenbauer, R.J., Koksalan, T., Palandri, J.L., 2005. Experimental investigation of CO2–brine–rock interactions at elevated temperature and pressure: implications for CO2 sequestration in deep-saline aquifers. Fuel Process. Technol. 86, 1581–1597. https://doi.org/10.1016/j.fuproc.2005.01.011.

Saleem, U., Wilhelms, A., Sottmann, J., Knuutila, H.K., Bandyopadhyay, S., 2025. Direct lithium extraction (DLE) methods and their potential in Li-ion battery recycling. Separ. Purif. Technol. 361, 131315. https://doi.org/10.1016/j.seppur.2024.131315.

Sass, E., Ben-Yaakov, S., 1977. The carbonate system in hypersaline solutions: dead sea brines. Mar. Chem. 5, 183–199. https://doi.org/10.1016/0304-4203(77)90006-8.

Scopus - analyze search results. https://www.scopus.com/term/analyzer.uri?sort=plf-f&src=s&sid=c3bb351aa8d513fb79f8126fd4749670&sot=a&sdt=a&sl=50&s=TITLE-ABS-KEY%28brine*+AND+chemical+AND+composition%29&origin=resultslist&count=10&analyzeResults=Analyze+results, 2025, 4.1.25.

Shah, K.M., Billinge, I.H., Chen, X., Fan, H., Huang, Y., Winton, R.K., Yip, N.Y., 2022. Drivers, challenges, and emerging technologies for desalination of high-salinity brines: a critical review. Desalination 538, 115827. https://doi.org/10.1016/j.desal.2022.115827.

Sharmin, T., Khan, N.R., Akram, M.S., Ehsan, M.M., 2023. A state-of-the-art review on geothermal energy extraction, utilization, and improvement strategies: conventional, hybridized, and enhanced geothermal systems. Int. J. Thermofluids 18, 100323. https://doi.org/10.1016/j.ijft.2023.100323.

Soltani, M., Moradi Kashkooli, F., Souri, M., Rafiei, B., Jabarifar, M., Gharali, K., Nathwani, J.S., 2021. Environmental, economic, and social impacts of geothermal energy systems. Renew. Sustain. Energy Rev. 140, 110750. https://doi.org/10.1016/j.rser.2021.110750.

Spitzer, P., Fisicaro, P., Meinrath, G., Stoica, D., 2011. pH buffer assessment and Pitzer's equations. Accred Qual. Assur. 16, 191–198. https://doi.org/10.1007/s00769-010-0743-0.

Stringfellow, W.T., Dobson, P.F., 2021. Technology for the recovery of lithium from geothermal brines. Energies 14, 6805. https://doi.org/10.3390/en14206805.

Tabelin, C.B., Dallas, J., Casanova, S., Pelech, T., Bournival, G., Saydam, S., Canbulat, I., 2021. Towards a low-carbon society: a review of lithium resource availability, challenges and innovations in mining, extraction and recycling, and future perspectives. Miner. Eng. 163, 106743. https://doi.org/10.1016/j.mineng.2020.106743.

Wigand, M., Carey, J.W., Schütt, H., Spangenberg, E., Erzinger, J., 2008. Geochemical effects of CO2 sequestration in sandstones under simulated in situ conditions of deep saline aquifers. Appl. Geochem. 23, 2735–2745. https://doi.org/10.1016/j.apgeochem.2008.06.006.

Williams, G.D.Z., Barre, J., Louvat, P., Bérail, S., Millot, R., Vengosh, A., 2026. Geochemical controls on the formation of lithium brines in closed-basins of the Lithium Triangle. Earth Planet Sci. Lett. 679, 119849. https://doi.org/10.1016/j.epsl.2026.119849.

Williams, G.D.Z., Nativ, P., Vengosh, A., 2025. The role of boron in controlling the pH of lithium brines. Sci. Adv. 11, eadw3268. https://doi.org/10.1126/sciadv.adw3268.

Williams, G.D.Z., Vengosh, A., 2025. Quality of wastewater from lithium-brine mining. Environ. Sci. Technol. Lett. 12, 151–157. https://doi.org/10.1021/acs.estlett.4c01124.

Xie, G., Guan, Q., Zhou, F., Yu, W., Yin, Z., Tang, H., Zhang, Z., Chi, R., 2023. A critical review of the enhanced recovery of rare Earth elements from phosphogypsum. Molecules 28, 6284. https://doi.org/10.3390/molecules28176284.

Xing, P., Wang, C., Chen, Y., Ma, B., 2021. Rubidium extraction from mineral and brine resources: a review. Hydrometallurgy 203, 105644. https://doi.org/10.1016/j.hydromet.2021.105644.

Zhou, Y., Fang, C., Fang, Y., Zhu, F., 2011. Polyborates in aqueous borate solution: a Raman and DFT theory investigation. Spectrochim. Acta Mol. Biomol. Spectrosc. 83, 82–87. https://doi.org/10.1016/j.saa.2011.07.081.